ADVANCED MATERIALS
www.advmat.de

Bioinspired Self-Healing Human–Machine Interactive Touch Pad with Pressure-Sensitive Adhesiveness on Targeted Substrates

Guorong Gao, Fangjian Yang, Fenghua Zhou, Jiang He, Wei Lu, Peng Xiao, Huizhen Yan, Caofeng Pan, Tao Chen,* and Zhong Lin Wang**

There is an increasing interest to develop a next generation of touch pads that require stretchability and biocompatibility to allow their integration with a human body, and even to mimic the self-healing behavior with fast functionality recovery upon damage. However, most touch pads are developed based on stiff and brittle electrodes with the lack of the important nature of self-healing. Polyzwitterion–clay nanocomposite hydrogels as a soft, stretchable, and transparent ionic conductor with transmittance of 98.8% and fracture strain beyond 1500% are developed, which can be used as a self-healing human–machine interactive touch pad with pressure-sensitive adhesiveness on target substrates. A surface-capacitive touch system is adopted to sense a touched position. Finger positions are perceived during both point-by-point touch and continuous moving. Hydrogel touch pads are adhered to curved or flat insulators, with the high-resolution and self-healable input functions demonstrated by drawing, writing, and playing electronic games.

Dr. G. Gao, Dr. W. Lu, Dr. P. Xiao, H. Yan, Prof. T. Chen
Key Laboratory of Marine Materials and Related Technologies
Zhejiang Key Laboratory of Marine Materials and Protective Technologies
Ningbo Institute of Materials Technology and Engineering
Chinese Academy of Sciences
Ningbo 315201, China
E-mail: tao.chen@nimte.ac.cn

Dr. G. Gao, Dr. J. He, Prof. C. Pan, Prof. Z. L. Wang
CAS Center for Excellence in Nanoscience
Beijing Key Laboratory of Micro-nano Energy and Sensor
Beijing Institute of Nanoenergy and Nanosystems
Chinese Academy of Sciences
Beijing 100083, China
E-mail: cfpan@binn.cas.cn

F. Yang
School of Aeronautics and Astronautics
University of Electronic Science and Technology of China
Chengdu 611731, China

F. Zhou
Unisoc Technologies Co., Ltd.
Shanghai 201203, China

Prof. Z. L. Wang
School of Materials Science and Engineering
Georgia Institute of Technology
Atlanta, GA 30332, USA
E-mail: zlwang@gatech.edu

The ORCID identification number(s) for the author(s) of this article can be found under https://doi.org/10.1002/adma.202004290.

DOI: 10.1002/adma.202004290

There is an increasing and considerable interest to develop integrated touch pads that provide a convenient human–machine interface for interacting with display devices.[1–6] Based on the several types of mechanisms such as resistive,[7,8] capacitive,[9,10] voltage,[2,5] etc., touch sensing has been used commonly in electronic devices such as mobile phones and ticketing machines. Although indium tin oxide (ITO) has been selected as a dominant transparent conducting film, the development of next generation of touch pads requiring stretchability, biocompatibility, and even self-healing to allow its integration with a human body, or with other various substrates in an easy adhesiveness, touch pads based on ITO face many challenges owing to their stiff and brittle nature.

As a general phenomenon of the self-healing behaviors among living species in nature, most organisms have the ability to self-healing upon encountering damages, and to retain the primary functionalities. Inspired by these, it is very important that developing touch pads to mimic the self-healing behavior could potentially allow them with fast functionalities recovery in a simple repairing process upon damages. As one of the well-known soft materials, there are a number of efforts have been presented to use polymeric hydrogel as an efficient candidate for use in flexible electronic devices[11] with promising possibilities as flexible electrodes,[12–15] sensors,[4,7–9,12,16,17] and displays[18,19] with the human body. The conductivity was achieved normally through the introduction of conductive polymers,[12,16] metal nanoparticles/nanowires,[2] carbon-based materials,[20] and soluble salt ions[21] into hydrogels. For example, Wu and co-workers reported a bioinspired hydrogel, composed of crosslinked poly(acrylic acid) and alginate chains by small calcium carbonate nanoparticles, was developed to fabricate a high sensitive, capacitive ionic skin sensor, which can sense the slightest change of pressure, such as a finger motion, a gentle touch, throat motion, and even blood pressure.[17] However, an important issue of transparence has been reduced sharply due to the introduction of insoluble calcium carbonate nanoparticles, which weakens the usefulness in touch pads. Sun and co-workers reported another strategy to achieve conductive yet transparent polyacrylamide (PAAm) hydrogels with dissolving lithium chloride

(LiCl) salts as the crucial component for the next generation of touch panels due to their stretchability, high ionic conductivity, and biocompatibility.[6] A surface-capacitive touch system was adopted for this panel to sense a touched position. However, the nature of covalently cross-linked PAAm hydrogel makes the absence of self-healing in this touch pad. Recently, transparent and conductive ionogels comprised of ionic liquids and polymers have been used as ionoskins to sense touch position,[22] force,[23] and monitor human movements,[24] with the biggest merit of no volatilization.[24] However, due to the absence of functional groups for bonding, these ionogels are nonadhesive, therefore, there is a need to be fixed on target surfaces with the help of tapes or glues. A key challenge for touch pad is to develop a single material system that combines transparency, conductivity, stretchability, biocompatibility, self-healing, and self-adhesive ability.

Herein, we developed polyzwitterion–clay nanocomposite hydrogels as a transparent ionic conductor, which could be used as a self-healing human–machine interactive touch pad with pressure-sensitive adhesiveness on various substrates. A surface-capacitive system was adopted for our ionic touch pad, in which the same voltage is applied to all corners of the pad, which results in a uniform electrostatic field across the pad. When a finger as conductor touches the pad, the touch point becomes grounded, and a potential difference is generated between the electrode and the touch point. The potential difference causes current to flow from the electrode through the finger. The magnitude of current is determined by the distance between the touch point and electrode. As the distance decreases, a larger current is induced. We use biocompatible polyzwitterion hydrogel network[25] including positively and negatively charged groups inside to provide a fast healing possibility. The equivalent cation and anion groups will promote the dispersion of nanoclays, which is essential to obtain high transparency as well as high stretchability.[26] Furthermore, the charged polar groups inside hydrogel network will generate weak polar interactions with pressure-sensitive adhesiveness to various solid substrates. Inorganic clays ($[Mg_{5.34}Li_{0.66}Si_8O_{20}(OH)_4]Na_{0.66}$, 20–30 nm in diameter, 1 nm in thickness) were used not only as reversible cross-linkers but also as the sources of mobile ions, because there are dissolved positive ions surrounding negatively charged clay platelets. Furthermore, the reversible polymer–clay crosslinking dissipate large amounts of energy during hydrogel extension or contraction, thus is essential for increasing the toughness of hydrogels.[27,28] The touch pads were demonstrated to adhere on plane and curved surfaces, and used to write words, draw figures, and play computer games both in original and cut-then-healed state.

The architecture of a 1D hydrogel touch strip is shown in **Figure 1**a. Each end of the strip is connected to a copper electrode and an external resistance (R_e), then connected to the same alternating current (AC) power. Same phase AC voltage (17 kHz, ±0.6 V) was applied through the two identical R_e to both ends of the strip. The electrical double-layer capacitance (C_{EDL}) is formed in electrode/hydrogel interface, because charges in the electrode and in the electrolyte are separated.[17] When a finger touches, a coupling capacitance (C_{finger}) formed in finger/hydrogel interface, allowing current to flow to finger and ground through human body. The hydrogel strip is a virtual resistance (R_h) and is divided into two parts by the finger, with the resistance value of each part proportional to its normalized length, i.e., x and $1–x$ in Figure 1a. The equivalent circuit is shown in Figure S1 (Supporting Information). Two parts of the hydrogel, xR_h and $(1–x)R_h$, are connected in parallel. In each parallel branch, the hydrogel resistance is connected with a C_{EDL} and a R_e in series. Voltages applied on the two parallel branches are equal, while applied on C_{EDL} is negligible because of high frequency (17 kHz) of AC voltage.[6] Thus, when the finger moves right, xR_h increases and the peak voltage from V1 meter (U_1) decreases, while $(1–x)R_h$ decreases and peak voltage on V2 meter (U_2) increases. Thereby, the finger position is reflected in one of the following equations

$$1 - x \propto U_1 \tag{1}$$

$$x \propto U_2 \tag{2}$$

The hydrogel networks are composed of polyzwitterions crosslinked by exfoliated nanoclays through reversible adsorption (Figure 1b), with mobile Na^+ ions originate from nanoclays as current carriers. The conductivity is 0.14 ± 0.01 S m^{-1} for hydrogels as measured by a four-probe method. The hydrogels are synthesized by in situ polymerization of 2 M 3-[dimethyl-[2-(2-methylprop-2-enoyloxy)ethyl]azaniumyl]propane-1-sulfonate (DMAPS) in aqueous solution of 6×10^{-2} M nanoclays, with 2×10^{-3} M ammonium persulfate (APS) as thermal initiator, but without addition of covalent cross-linkers. As illustrated in Figure 1b, when two freshly cut hydrogel sections are put together, the dangling chains near surfaces contact first, forming electrostatic attractions between zwitterion groups, leading to a quick interfacial adhesion and rebuilding of ionic channels. Then, the polymer chains further diffuse, until bridging of the adjacent nanoclays[29] occurs across the interface (Figure 1c), which leads to the increase of healing efficiency.[30]

The polar zwitterion groups provide active sites to form noncovalent bonding, such as hydrogen bonds, electrostatic attractions, and ion–polar interactions to various substrates. For example, upon contact with human skin, the sulfonic acid groups may form hydrogen bonding and electrostatic attraction with the tissues[31,32] (Figure 1d), leading to hydrogel–skin adhesion (Figure 1e). Besides, in contrast to polymer chains that are separated by crosslink points in covalently crosslinked hydrogels, the long polymer chains are intact in our polyzwitterion–clay hydrogels, which is beneficial to form continuous noncovalent bonding along chains[33,34] and strong hydrogel–substrate adhesion. Therefore, the hydrogels are pressure-sensitive adhesive to plastics, rubbers, fibers, and other materials, which is a feature essential for integration to electronics devices and wearable applications.

We demonstrated the position-sensing function of a 1D hydrogel strip. A touch strip was point-by-point touched from left (x = 1/15) to right (x = 14/15), with the step length of x = 1/15 (Figure 1f). Before touch, the baseline voltage is generated for the presence of leakage current from hydrogel to environments.[6] Upon touch, additional touch voltage occurred. From x = 1/15 to x = 14/15, the peak V1 voltage linearly decreased (Figure 1f), while peak V2 voltage linearly increased (Figure S2, Supporting Information), which is, respectively, in accordance with Equations (1) and (2), indicating the touch

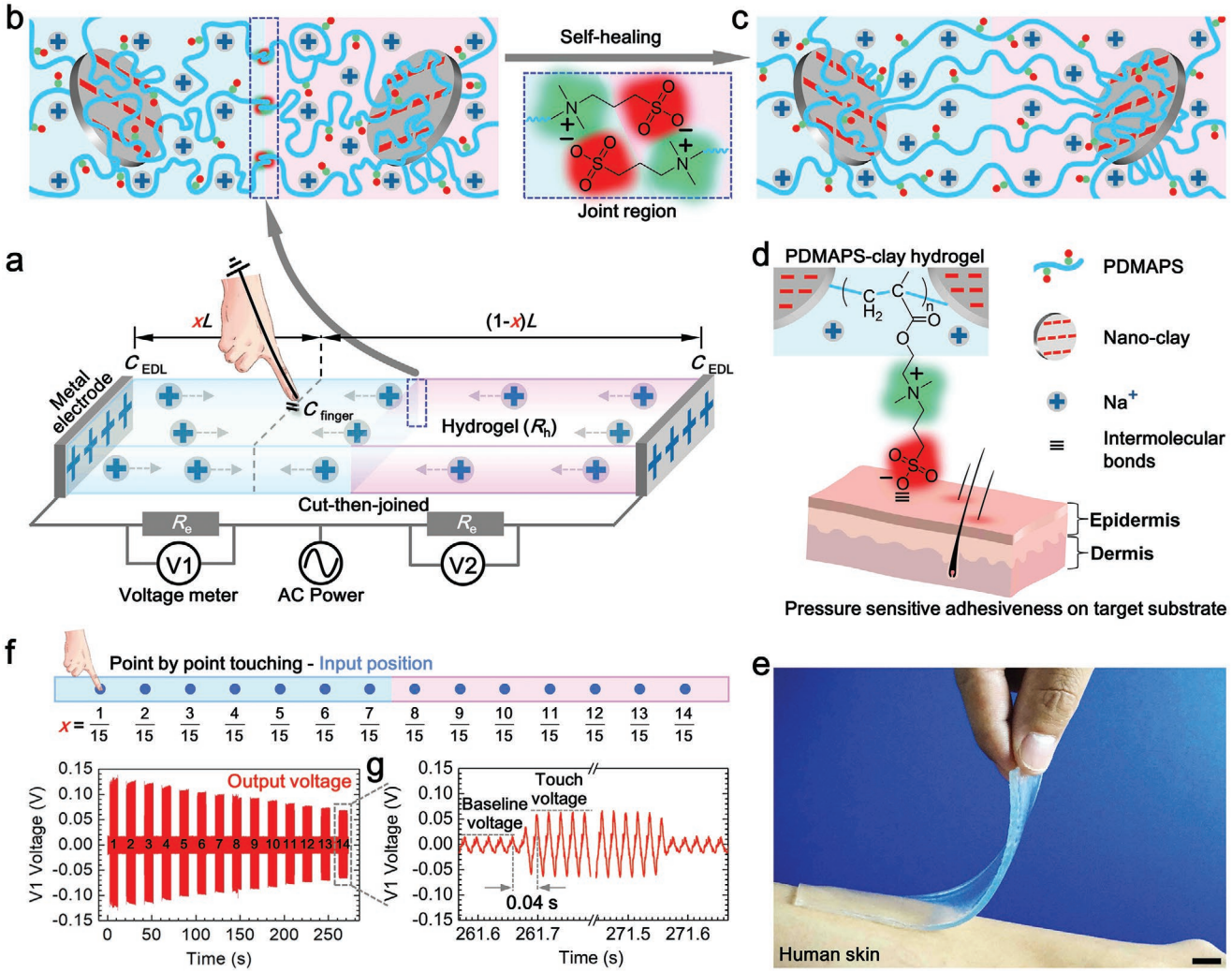

Figure 1. Position sensing on self-healing and adhesive polyzwitterion–clay nanocomposite hydrogels. a) The architecture of 1D hydrogel touch strip. b,c) Schemes illustrating cut hydrogels healed by electrostatic attraction between polyzwitterions (b) and rebuilding polyzwitterion–clay adsorption (c). d) Schematic illustration of hydrogels adhered to the skin through intermolecular bonds. e) A photo of a hydrogel adhered to human skin. f) A finger point-by-point touching on a hydrogel strip from $x = 1/15$ to 14/15, and corresponding V1 voltage recorded by time. g) The detailed AC voltage signals when point 14 was touched. Scale bar in (e): 1 cm.

strip could be used to input changed position information. The detected AC frequency (50 Hz) is much less than the frequency (17 kHz) generated from AC power, because there is an upper limit of the sampling frequency of voltage meter (25 kHz). The hydrogels still have position-sensing functions after gradual drying. A hydrogel strip exposed in ambient condition (25 °C, 56% RH) was weighed and point-by-point touched at determined time until 120 h; the measured voltages and weights at each time are plotted and labeled in Figure S3 (Supporting Information). The touching voltage is sufficient to be detected at each point-by-point touching cycle, and the detected peak V2 voltage always monotonously increased as the finger moved from $x = 0.2$ to 0.5 to 0.8. The baseline voltage decreased from 0.03 to 0.007 V in 120 h (Figure S3, Supporting Information), which is suspected to be related to drying of hydrogel and reduced charges leakage from hydrogel to enviroments.

To provide comfortable touch feeling and avoid water evaporation, we covered the hydrogels with 100 µm thick poly(dimethylsiloxane) (PDMS) films. With the presence of PDMS, C_{finger} still exists, and a hydrogel strip still shows finger location ability (Figure S4, Supporting Information). To achieve seamless PDMS–hydrogel adhesion, the hydrogels were synthesized on PDMS surfaces. Briefly, PDMS films were fixed on inner surfaces of glass molds, then the hydrogel precursors were injected followed by polymerization (Figure S5, Supporting Information). The seamless film–hydrogel contact and the polar groups in hydrogel ensured the stable PDMS–hydrogel adhesion. From lap sheer and 90° peeling-off test, the shear strength and interfacial toughness of PDMS–hydrogel adhesion is 3.9 kPa (Figure S6a, Supporting Information) and 73 J m^{-2} (Figure S6b, Supporting Information), respectively. During peeling off PDMS, the hydrogel was lifted away from table by adhesion force (Figure S6c, Supporting Information). The PDMS-covered

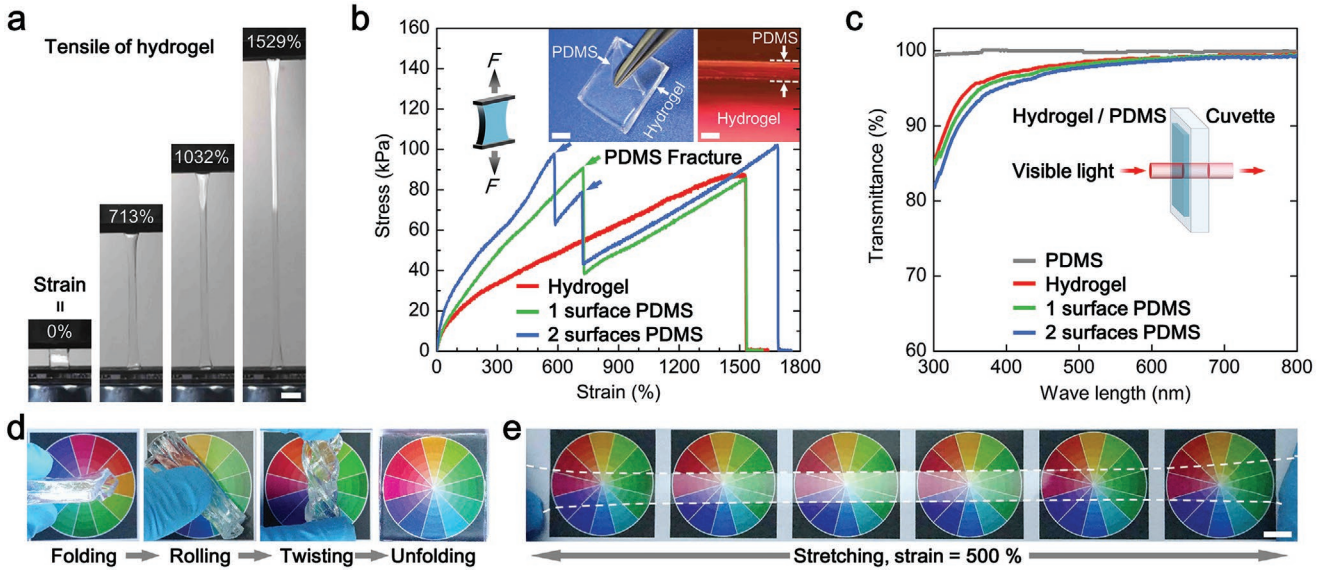

Figure 2. Stretchability and transparency of hydrogels and PDMS-covered hydrogels. a) Photos recording the tensile process of a hydrogel. b) Stress–strain curves of hydrogels and PDMS-covered hydrogels. Insets: left, a photo showing a PDMS film peeling from a hydrogel; right, optical microscopy image of a PDMS-covered hydrogel. c) Transmittance spectra of PDMS, hydrogel, and PDMS-covered hydrogels. d) Photos of a PDMS-covered hydrogel that is subjected to successive folding, rolling, twisting, and then unfolding. e) Another PDMS-covered hydrogel is stretched to strain of 500%. Scale bars: 100 μm for right inset in (b) and 1 cm for the rest.

hydrogels show obvious lower water loss rate than that of bare hydrogels, as reflected from the weight–time curves (Figure S7a, Supporting Information) and size change by time of samples stored in desiccator (Figure S7b, Supporting Information), indicating PDMS covered on hydrogel surface is effective in delaying the evaporation of hydrogels.

The transparent hydrogels could be stretched to strain beyond 1500% (**Figure 2**a,b), with fracture stress of 88 kPa (Figure 2b), and show average transmittance of 98.8% in wavelength range of 400–800 nm (Figure 2c). The fracture stain of PDMS is 696% ± 121% (Figure S8, Supporting Information). During tensile test of PDMS-covered hydrogels, PDMS first fractured at strains of 580–721% (Figure 2b), then hydrogels were steadily elongated until fracture. The hydrogels with one and two surfaces covered by PDMS show average transmittance of 98.6% and 98.2%, respectively. The PDMS-covered hydrogel is highly transparent even after folding, rolling, twisting, and then unfolding (Figure 2d), or at strain of 500% (Figure 2e). The high stretchability and transparency make the hydrogels and PDMS-covered hydrogels suitable for using as soft touch pads.

The hydrogels are pressure-sensitive adhesive to various solid surfaces. Movie S1 (Supporting Information) shows the hydrogel pieces adhere to flat or curved insulation substrates including filter paper, glass, nitrile rubber, wood, cotton fabric, poly(ethylene terephthalate) (PET), acrylonitrile butadiene styrene (ABS), VHB tape, silicone rubber, nylon, poly(methyl methacrylate) (PMMA), polystyrene (PS), and polyethylene (PE) through attach and gentle press. The adhered hydrogel pieces support their weights rather than creeping down (**Figure 3**a and Movie S1, Supporting Information). We evaluated the hydrogel–substrate adhesion properties through lap sheer (Figure 3b and Figure S9a, Supporting Information) and 90° peeling-off (Figure 3c and Figure S9b, Supporting Information) tests, and summarized the shear strength and interfacial toughness of these hydrogel–substrate adhesions (Figure 3d). The interfacial toughness of hydrogels to filter paper, glass, and nitrile rubber is between 418 ± 38 and 318 ± 11 J m^{-2}, comparable with that of covalent bonding between tough hydrogels and porcine heart (340 J m^{-2}).[32] Hydrogels undergo cohesive failure during peeling from these substrates. The interfacial toughness is between 288 ± 13 and 38 ± 4 J m^{-2} of hydrogels to wood, cotton fabric, PET, ABS, VHB tape, silicone rubber, nylon, PMMA, PS, and PE. Hydrogels undergo adhesion failure during peeling and is reversible adhesive to these substrates.

Strong adhesion needs the synergy of chemical bonding, topology of connection,[31,35] and energy dissipation in crack zone of hydrogels.[32,36,37] Possible chemical bonding between hydrogels and filter paper, glass, nitrile rubber, wood, cotton fabric, PET, ABS, silicon rubber, and nylon includes H-bonds, ion–dipole interactions, cation–π interactions, and electrostatic attractions (Figure S10, Supporting Information). While, polymer chains in hydrogels may penetrate into porous substrate surfaces, such as open pores in paper and cotton fabric (Figure S11a, Supporting Information) and closed pores on glass surface (Figure S11b, Supporting Information) to increase contact areas. Besides, the reversible polymer–clay adsorptions and electrostatic attractions between zwitterions in hydrogels provide dissipation mechanism, and result in additional energy needed for propagation of interfacial crack. Therefore, the strong hydrogel–substrate adhesion could be explained by a synergy mechanism. For instance, polymers in hydrogel will penetrate into filter paper pores to form abundant H-bonds and even entanglements with cellulose fibers, while hydrogel dissipates energy near crack zone through breaking of noncovalent crosslinking, thus resulting in a high interfacial toughness (418 ± 38 J m^{-2}) of hydrogel–filter paper adhesion.

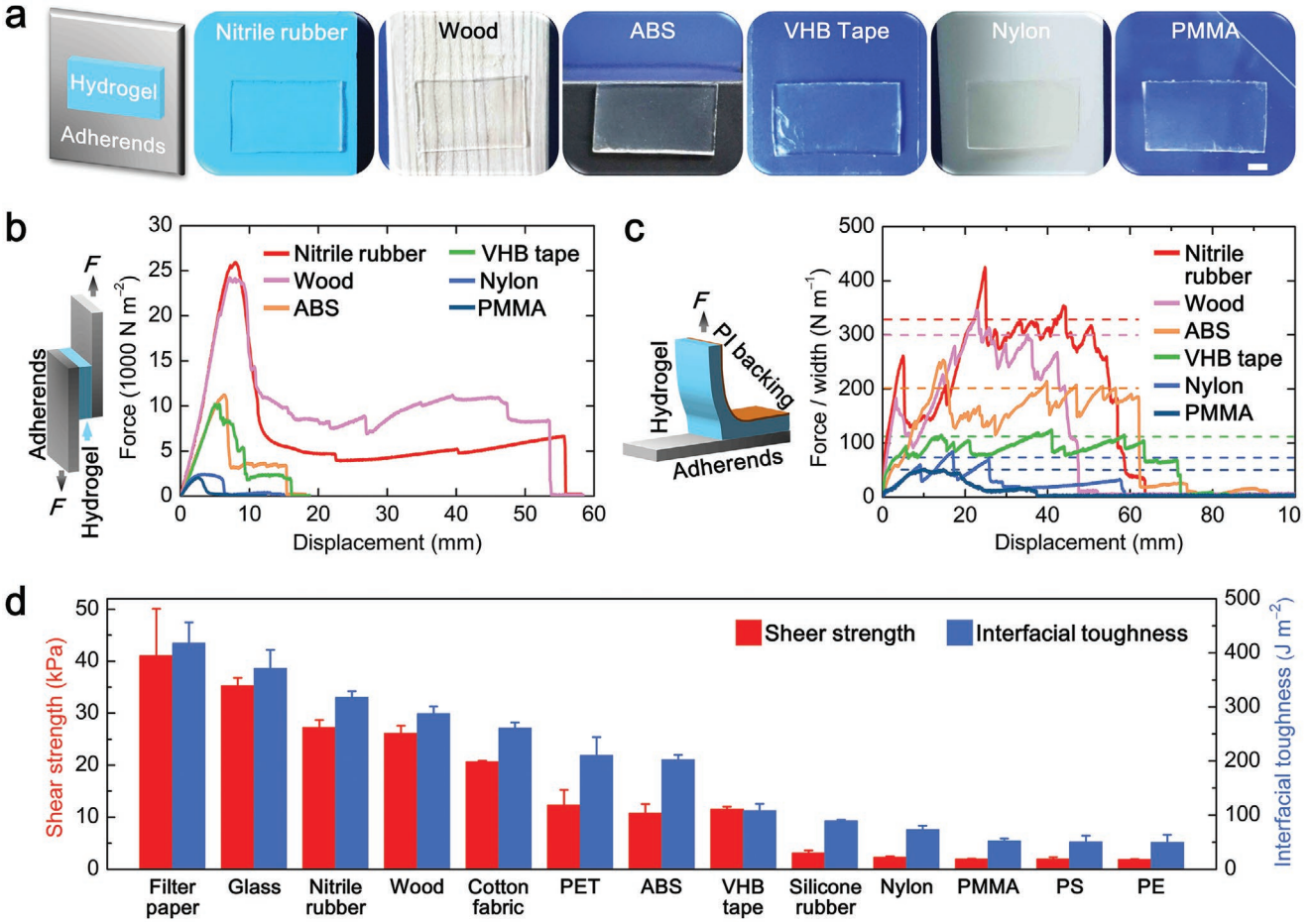

Figure 3. Pressure-sensitive adhesion of hydrogels. a) Photos of hydrogels adhered on nitrile rubber, wood, ABS, VHB tape, nylon, and PMMA. b) Lap sheer and c) 90° peeling-off curves of hydrogels adhered to above materials. d) Shear strength and interfacial toughness of hydrogels adhered to various solid substrates. Error bars indicate the standard deviation for $n = 3$ measurements. Scale bar in (a): 1 cm.

Weak adhesion, such as adhesion of hydrogels to the smooth and compact nylon, PMMA, PS, and PE surfaces, may be dominated by weak interfacial polar and van der Waals interactions. The weak adhesion avoids large-scale deformation, shear lag, and mechanical damage during peeling off, which is crucial for repeat adhesion. Movie S2 (Supporting Information) shows the hydrogels were smoothly peeled off from nylon rod and PMMA panel during repeat pressure-sensitive adhesion.

The mechanical properties and electrical conductivity of hydrogels are self-healable. The tensile properties of cut-then-joined hydrogels gradually recovered by prolonging storage time in PE seal film (**Figure 4**a). Right after cut-then-join, the hydrogels can be stretched to a strain of 323% and stress of 7.2 kPa. After being healed at 25 °C for 24 h, the hydrogel shows a maximum tensile strain of 1492% and stress of 63.5 kPa, close to that of unbroken hydrogel, with a healing efficiency of 98% in terms of fracture strain. Figure 4b shows two newly cut sections were seamlessly integrated together right after join, then bear stretching. The instantaneous healing rebuilds ion channels in hydrogels, leading to recovery of electrical conductivity. As shown in Figure 4c, the direct current in a cut-then-joint hydrogel recovered in 21 s.

The finger location function of hydrogels also recovered after self-healing. We moved a finger on a PDMS-covered hydrogel touch strip from $x = 0$ to 1 at an approximately constant speed (Figure 4d). The recorded peak V1 voltage continuously and linearly decreased by time. When the same strip was cut and then joined, moving a finger on it still resulted in continuous and linear change of peak V1 voltage (Figure 4e). A touch strip was used to play a piano game, both before and after cut-then-join. The strip was self-adhered to a nylon rod. A well-known song, jingle bells, was played by touching the note positions labeled behind hydrogel (Movie S3, Supporting Information). When playing, the generated touch voltage was recorded (Movie S4, Supporting Information) and synchronously converted to corresponding video and audio signals by a computer. Next, we cut off the strip, then join the cut surfaces together (Figure 4f). The healed strip recovered its input function as proved by playing the same song (Figure 4g and Movie S5, Supporting Information).

To feel the finger location, we performed experiments to locate a finger on 2D touch pads. As shown in **Figure 5**a, each corner of a square hydrogel was connected to a metal electrode, and then connected to a R_e in series. The four R_e were

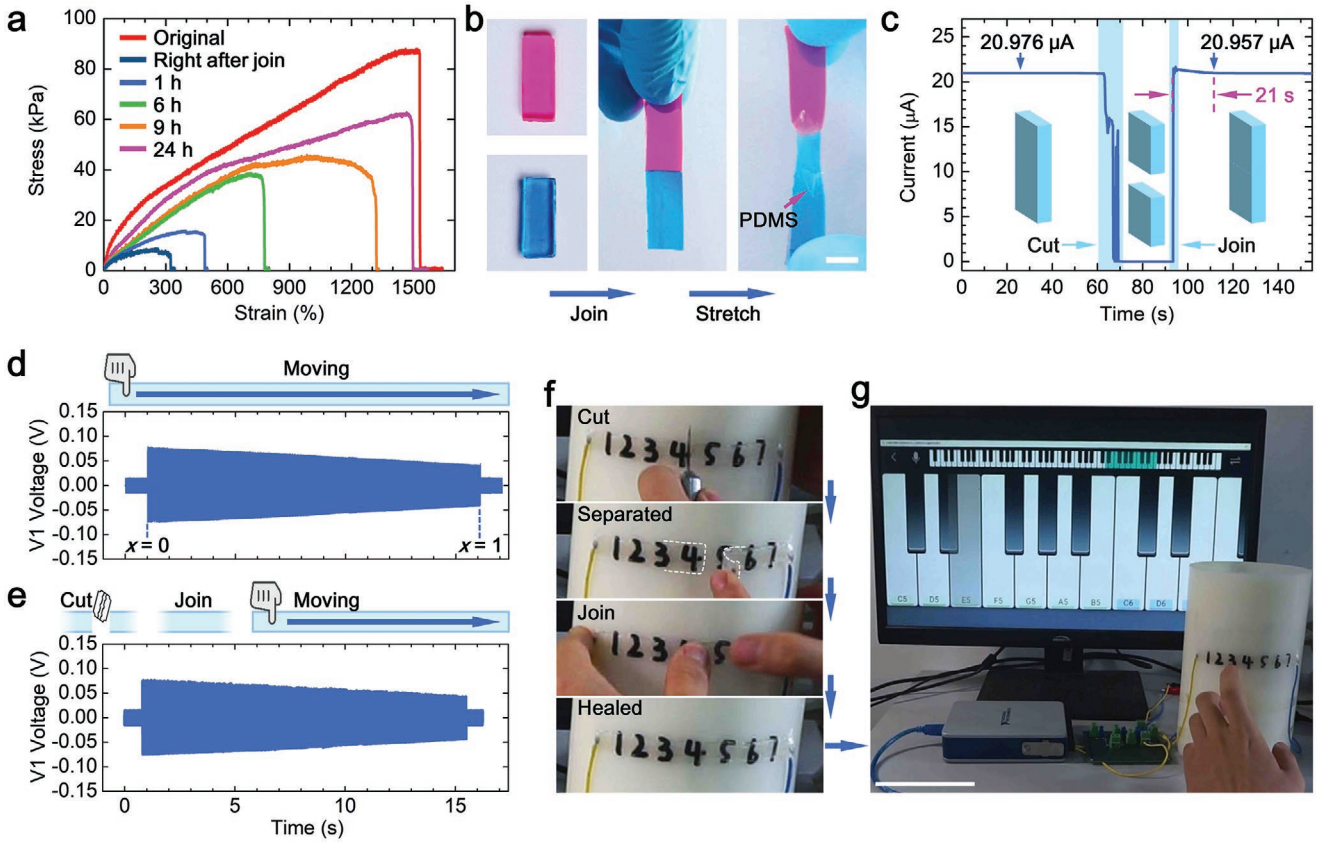

Figure 4. Self-healing and operation of a 1D touch strip. a) Stress–strain curves of hydrogel and hydrogels healed for different times. b) Photos of two freshly cut hydrogel sections joint together and stretched by hands. c) The current in a hydrogel varied by time, when it was intact, cut, and joined. d,e) The V1 voltage recorded by time when a finger moved on the original (d) and the cut-then-rejoined (e) touch strips. f) A touch strip adhered on a nylon rod was cut then joined, and g) used to play a piano game. Scale bars: 1 cm in (b) and 10 cm in (g).

connected to a same AC power in parallel. The voltage on each R_e was measured through an independent voltage meter. The position-sensing mechanism of a 2D pad is identical to that of a 1D strip: when a finger touches, the voltage on a certain R_e is inversely proportional to the corresponding finger–corner distance. To verify this mechanism, we point-by-point touched 17 points along the diagonal lines of a 2D hydrogel touch pad (Figure 5a), and recorded the V1, V2, V3, and V4 voltages by time (Figure S12, Supporting Information). Figure 5b shows the peak voltages (U_1, U_2, U_3, and U_4) of these touch points. When a finger moves far away from a voltage meter, the corresponding peak touch voltage decreases. For example, when the finger moved from point 1 to 9, U_1 decreased from 0.0131 to 0.009 V; subsequently, the finger moved from point 10 to 13, U_1 increased from 0.0104 to 0.011 V; then, the finger moved from point 14 to 17, U_1 decreased from 0.011 to 0.0101 V. On the other hand, for a certain touch point, the U_1, U_2, U_3, and U_4 are inversely proportional to the corresponding corner–finger distance. For example, the U_1, U_2, U_3, and U_4 of point 2 are 0.0129, 0.0112, 0.01, and 0.0112 V (Figure 5b), respectively, and they match with the normalized distance of point 2 to V1, V2, V3, and V4 corner (Figure 5a), 0.18, 0.88, 1.24, and 0.88, respectively.

As analyzed above, the finger position (x, y) on a 2D touch pad can be determined by the same method used in a 1D touch strip. Briefly, if we treat the 2D pad as a horizontal 1D strip, the x (in Figure 5a) will be determined by

$$x \propto \frac{U_3 + U_4}{U_1 + U_2 + U_3 + U_4} \tag{3}$$

Similarly, if the 2D pad is treated as vertical 1D, the y (in Figure 5a) will be determined by

$$y \propto \frac{U_2 + U_3}{U_1 + U_2 + U_3 + U_4} \tag{4}$$

Based on Equations (3) and (4), we calculated the output positions corresponding to touch points in Figure 5a, and show them in Figure 5c. The U_1, U_2, U_3, and U_4 values used for calculation are listed in Table S1 (Supporting Information). Detailed calculation procedure is shown in Equations (S1)–(S6) (Supporting Information). From Figure 5c, the output positions well match the input positions (Figure 5a) in a macroscopic view. Indicating the 2D hydrogel touch pads could be used to input finger position.

We integrate the touch pad onto a LCD monitor to make a touch screen (Figure 5d). A square piece of PDMS-covered hydrogel was self-adhered to a PMMA plate that was fixed on a monitor. Metal electrodes connected to hydrogel corners were

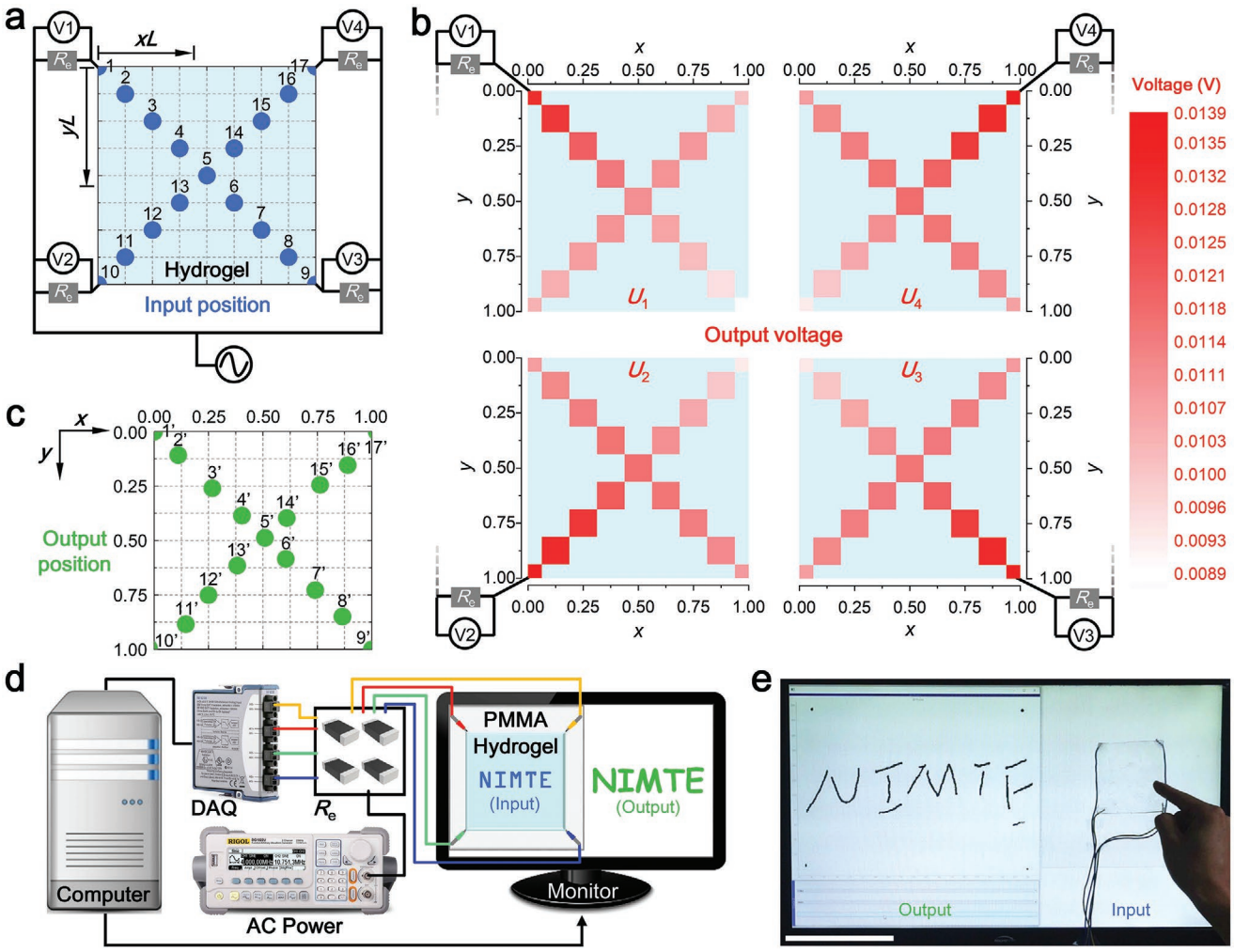

Figure 5. Finger location and operation of 2D touch pads. a) A schematic diagram of a 2D touch pad labeled with 17 input positions. b) Peak voltage detected by V1, V2, V3, and V4 meters during a finger touch above positions. c) The calculated output positions. d) The diagram of an integrated hydrogel touch screen. e) A photo shows the touch screen was used to write abbreviations NIMTE of Ningbo Institute of Materials Technology and Engineering. Scale bar in (e): 10 cm.

inserted in hydrogel–PMMA interface. Each hydrogel corner was connected to a R_e. The four R_e connected to the same AC power in parallel. Voltages applied on each R_e were collected through an independent channel in a data acquisition card (DAQ), which is connected to a computer (Figure 5d). During finger touch, the real-time V1, V2, V3, and V4 voltages are converted into digital signals by the DAQ and transmitted to a computer. The computer calculates and synchronously displays the finger position on the same monitor (Figure 5d). Thereby, one could write or draw on the touch screen. We use the integrated touch screen to write words NIMTE (Figure 5e and Movie S6, Supporting Information) and draw a smile face (Movie S7, Supporting Information). High-resolution words and images are observed, which are in sharp contrast to previously reported low-resolution and fuzzy images generated from touch pads based on sensor array.[38,39] The resolution of a sensor array is determined by the number of array points per unit area. However, polymer materials are incompatible with standard photolithography microfabrication technology, making it highly challenging to produce high-density sensor arrays.[1] The reported sensor array based polymer touch pads show resolutions ranging from 1 array point per 10 cm^2[40] to 1 array point per 1 cm^2 area.[41,42] In contrast, the finger position on our hydrogel touch pad is calculated from voltages on four external resistances. In theory, the resolution of the surface capacitive touch pad is infinitely high.

The touch screen is self-healable. In Movie S8 (Supporting Information), two concentric squares were drawn on the touch screen through tracing the patterns behind the hydrogel. Then, a crack was cut on the hydrogel, followed by joining together for healing (Movie S9, Supporting Information). After 1 min, we successfully drew two concentric squares through tracing the same patterns again.

Based on the 2D location of the polymeric hydrogel touch pad, we performed further experiments to use the touch pad as wearable input device. VHB 4910 tape was used as insulating spacer between hydrogel and human body. A PDMS-covered hydrogel was adhered on the tape surface. Then, metal wires

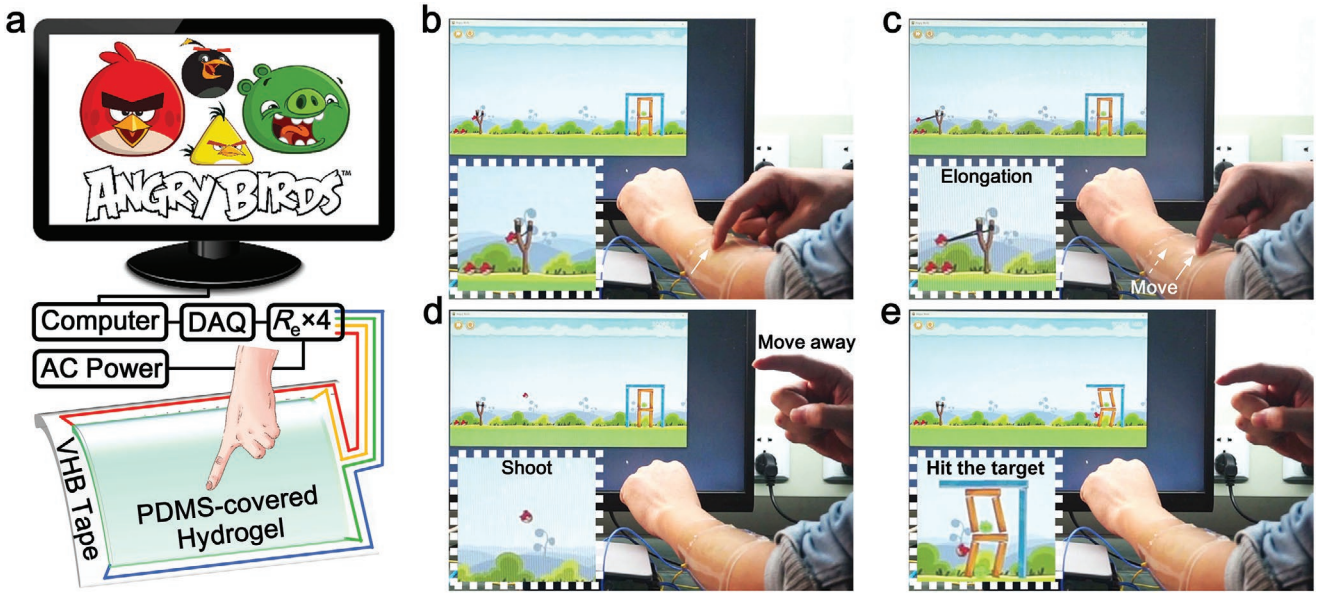

Figure 6. Operation of a wearable touch pad. a) A schematic diagram of a wearable touch pad integrated into a personal computer system, and used to play the Angry Birds game. b–e) Photos record when: a slingshot loaded with an Angry Bird was activated when finger touched the pad (b), the slingshot was gradually pulled back when the finger moved on the touch pad (c), the bird was launched when the finger moved away (d), and the bird hit the target (e). The insets in (b)–(e) show the area near birds enlarged for clarity. Scale bar: 10 cm. Angry Birds graphical material is used with permission of Rovio Entertainment Corporation. No further reproductions of this material are permitted.

were inserted into tape–hydrogel interface at four corners, and connected the hydrogel to computer (**Figure 6**a). We wear the touch pad on arm, and used to play a famous electronic game angry birds. The touch pad was conformally adhered on the arm (Figure 6b), which benefitted from the soft feature of VHB tape, hydrogel, and PDMS. The slingshot in the game was activated when a finger touches any position on touch pad (Figure 6b). The slingshot carried with a bird was elongated and tensioned by moving finger on touch pad (Figure 6c). During finger moving, the finger position was recorded by computer, and the moving length was calculated, which was transformed as elongated length of slingshot. When the finger moved away, the bird was launched upward (Figure 6d), and subsequently hit a target (Figure 6e and Movie S10, Supporting Information).

In summary, we have developed a self-healing, pressure-sensitive adhesive, transparent and highly stretchable nanocomposite hydrogel ionic conductor, and realized position sensing on it by adopting the surface capacitive touch (SCT) technology. The hydrogel networks are composed of polyzwitterions crosslinked by Laponite nanoclays (Laponite is a trademark of BYK Additives Ltd.). Because of noncovalent crosslinking and presence of polar zwitterion groups, the cut-then-joined hydrogel recovers its ionic conductivity in 21 s, and the hydrogels are pressure-sensitive adhesive to various insulating materials including cotton fabric, ABS, silicone rubber, PMMA, etc. In SCT system, the detected voltage precisely reflected the finger positions on hydrogel. The hydrogels self-adhered on curved nylon rod, flat PMMA, and worn on human arm were integrated into computers and used as touch pads for writing, drawing, and playing computer games both in original and self-healing state. The scientific concept and disruptive technology demonstrated here open up possibility for utilization of polymeric nanocomposite hydrogels as flexible human–machine communication interfaces with self-healing nature.

Experimental Section

Materials: Synthetic nanoclay Laponite XLG (trademark) was obtained from BYK Additives & Instruments. DMAPS, APS, rhodamine B, and methylene blue were purchased from Sinopharm Chemical Reagent Co., Ltd. PDMS film was purchased from Hangzhou Bald Advanced Materials Co., Ltd. VHB 4910 tape (1 mm thickness) was obtained from 3M Corporation. Deionized water (18.2 MΩ at 25 °C) was used in all experiments.

Synthesis of Hydrogels: Nanoclays (4.572 g, 6×10^{-2} M) were dissolved in water (100 mL), followed by sonication for 30 min for exfoliation. Next, DMAPS (55.87 g, 2 M) was added and stirred for 2 h. Subsequently, APS (0.046 g, 2×10^{-3} M) was added and stirred for another 10 min. The transparent solution was injected into a flat PMMA mold. The hydrogel was obtained after polymerization at 45 °C for 48 h. Rhodamine B (0.02 g L^{-1}) or methylene blue (0.02 g L^{-1}) was, respectively, added to synthesize red or blue hydrogels.

To fabricate PDMS-covered hydrogels, the PDMS film attached on PET liner was fixed on flat glass, and exposed to the assembled mode chamber (Figure S5, Supporting Information). Thereby, the injected solution was seamlessly contacted with PDMS. After polymerization, PDMS-covered hydrogel was obtained through removing glasses and peeling off PET.

90° Peeling-Off Tests: Peeling tests were performed on an Instron 5567 testing machine equipped with a 200 N load cell.

The substrate was fixed on the testing machine. As a stiff backing, PI film was bonded onto hydrogel by using cyanoacrylate adhesives. 2 cm length of hydrogel was prepeeled from the substrate and clamped to the testing machine. Before peeling, the initial hydrogel–substrate contact area was fixed at 10 cm × 1.5 cm.

The tests were conducted at a constant peeling speed of 50 mm min^{-1}. Interfacial toughness is determined through dividing the plateau force by the width of the hydrogel. In some cases, there is no plateau force, the maximum force was used to calculate the interfacial toughness.

Lap Sheer Tests: A hydrogel (1.5 cm × 1.5 cm) was sandwiched between two substrates (1.5 cm × 4.5 cm). As stiff backings, PI films were bonded to elastomer substrates such as nitrile rubber. The adhered assemblies were loaded to testing machine. All tests were conducted at a speed of 50 mm min^{-1}. Shear strength is determined as the maximum force per unit area.

Tensile Tests: Tensile tests were performed at 25 °C and 56% relative humidity (RH). Strip samples (width 1 cm and thickness 3 mm) were loaded to Instron 5567 machine, with an initial gauge length of 1 cm, and elongated at a speed of 10 mm min^{-1}. The tensile strain (ε) was defined as $\varepsilon = (l - l_0)/l_0 \times 100\%$, where l is the length and l_0 is the initial gauge length. The tensile stress (σ) was defined as $\sigma = F/A_0$, where F is the load and A_0 is the initial cross-sectional area.

To measure the tensile properties of self-healed hydrogels, the samples were cut into two sections, followed by subsequent joining of the cut surfaces together. The joined hydrogels were sealed in PE films for determined time.

Optical Microscopy Measurements: Optical microscopy image of PDMS-covered hydrogel was obtained on a digital microscope camera (Leica DFC450 C).

Transmittance Measurements: The optical transmittance was measured on an UV/vis spectroscopy (Lambda 950, Perkin-Elmer) in 300–800 nm range, and the tests were conducted at 25 °C and 56% RH, without considering the reflectance. The thickness of hydrogel samples is 3 mm.

Electrical Property Measurements: The conductivity of hydrogels was measured by using a digital four-probe tester (ST-2258C, Suzhou Jingge Electronic Co., Ltd.).

To measure the DC current in hydrogel before and after self-healing, a PDMS-covered hydrogel with size of 15 cm × 2 cm × 0.32 cm was connected to an electrochemical workstation (CHI600E, ChenHua Instruments Co., Ltd.). Voltage of 0.1 V was applied on the hydrogel. The strip was cut by a sharp knife. Then, the freshly cut surfaces were joined together. In the whole process, the DC current was recorded by time.

Touch Strip: Each end of a hydrogel strip (15 cm × 2 cm × 0.3 cm) was connected to an external resistance (R_e, 47 kΩ) by copper wire. An AC power (DG 1022U, RIGOL) was connected to both R_e. The voltage used was ±0.6 V, 17 kHz. Voltage on each R_e was collected through an independent channel in a DAQ (NI 9238, National Instruments). A software, DAQ-express, was used to read the voltage signals by time.

Touch Pad: Four corners of a hydrogel (8 cm × 8 cm × 0.3 cm) were, respectively, connected to a copper wire, which was then connected to a R_e (64 kΩ). The four R_e were connected to the same AC power in parallel. AC voltage of ±0.6 V and 17 kHz were used. The voltage on each R_e was collected by a DAQ.

Supporting Information

Supporting Information is available from the Wiley Online Library or from the author.

Acknowledgements

G.G. and F.Y. contributed equally to this work. This work was supported financially by National Natural Science Foundation of China (51773215, 21774138, 61675027, 51622205, 51432005, 61805015, and 61804011), Key Research Program of Frontier Sciences, Chinese Academy of Sciences (QYZDB-SSW-SLH036), Youth Innovation Promotion Association of Chinese Academy of Sciences (2019297), Open Research Fund of Key Laboratory of Marine Materials and Related Technologies (2018K02), Beijing City Committee of Science and Technology (Z171100002017019 and Z181100004418004), Natural Science Foundation of Beijing Municipality (4181004, 4182080, 4184110, 2184131, and Z180011), National Key R&D project from Minister of Science and Technology, China (2016YFA0202703 and 2016YFA0202704), and Shenzhen Science and Technology Program (Grant No. KQTD20170810105439418).

Conflict of Interest

The authors declare no conflict of interest.

Keywords

adhesiveness, hydrogels, ionic conductors, self-healing, touch pads

Received: June 24, 2020
Revised: August 17, 2020
Published online:

[1] S. Wang, J. Xu, W. Wang, G.-J. N. Wang, R. Rastak, F. Molina-Lopez, J. W. Chung, S. Niu, V. R. Feig, J. Lopez, T. Lei, S.-K. Kwon, Y. Kim, A. M. Foudeh, A. Ehrlich, A. Gasperini, Y. Yun, B. Murmann, J. B. H. Tok, Z. Bao, *Nature* **2018**, *555*, 83.
[2] X. Wang, Y. Zhang, X. Zhang, Z. Huo, X. Li, M. Que, Z. Peng, H. Wang, C. Pan, *Adv. Mater.* **2018**, *30*, 1706738.
[3] X.-Q. Wang, C.-F. Wang, Z.-F. Zhou, S. Chen, *Adv. Opt. Mater.* **2014**, *2*, 652.
[4] Z. Lei, P. Wu, *Mater. Horiz.* **2019**, *6*, 538.
[5] Y. Lee, S. H. Cha, Y.-W. Kim, D. Choi, J.-Y. Sun, *Nat. Commun.* **2018**, *9*, 1804.
[6] C.-C. Kim, H.-H. Lee, K. H. Oh, J.-Y. Sun, *Science* **2016**, *353*, 682.
[7] X. Yu, Z. Xie, Y. Yu, J. Lee, A. Vazquez-Guardado, H. Luan, J. Ruban, X. Ning, A. Akhtar, D. Li, B. Ji, Y. Liu, R. Sun, J. Cao, Q. Huo, Y. Zhong, C. Lee, S. Kim, P. Gutruf, C. Zhang, Y. Xue, Q. Guo, A. Chempakasseril, P. Tian, W. Lu, J. Jeong, Y. Yu, J. Cornman, C. Tan, B. Kim, K. Lee, X. Feng, Y. Huang, J. A. Rogers, *Nature* **2019**, *575*, 473.
[8] G. Ge, Y. Zhang, J. Shao, W. Wang, W. Si, W. Huang, X. Dong, *Adv. Funct. Mater.* **2018**, *28*, 1802576.
[9] Z. Lei, P. Wu, *Nat. Commun.* **2019**, *10*, 3429.
[10] J.-Y. Sun, C. Keplinger, G. M. Whitesides, Z. Suo, *Adv. Mater.* **2014**, *26*, 7608.
[11] Q. Rong, W. Lei, M. Liu, *Chem. Eur. J.* **2018**, *24*, 16930.
[12] Q. Rong, W. Lei, L. Chen, Y. Yin, J. Zhou, M. Liu, *Angew. Chem., Int. Ed.* **2017**, *56*, 14159.
[13] C. H. Yang, B. Chen, J. J. Lu, J. H. Yang, J. Zhou, Y. M. Chen, Z. Suo, *Extreme Mech. Lett.* **2015**, *3*, 59.
[14] T. B. H. Schroeder, A. Guha, A. Lamoureux, G. VanRenterghem, D. Sept, M. Shtein, J. Yang, M. Mayer, *Nature* **2017**, *552*, 214.
[15] C. Keplinger, J.-Y. Sun, C. C. Foo, P. Rothemund, G. M. Whitesides, Z. Suo, *Science* **2013**, *341*, 984.
[16] G. Ge, Y. Lu, X. Qu, W. Zhao, Y. Ren, W. Wang, Q. Wang, W. Huang, X. Dong, *ACS Nano* **2020**, *14*, 218.
[17] Z. Lei, Q. Wang, S. Sun, W. Zhu, P. Wu, *Adv. Mater.* **2017**, *29*, 1700321.
[18] C. H. Yang, S. Zhou, S. Shian, D. R. Clarke, Z. Suo, *Mater. Horiz.* **2017**, *4*, 1102.
[19] C. Larson, B. Peele, S. Li, S. Robinson, M. Totaro, L. Beccai, B. Mazzolai, R. Shepherd, *Science* **2016**, *351*, 1071.
[20] C.-R. Chen, H. Qin, H.-P. Cong, S.-H. Yu, *Adv. Mater.* **2019**, *31*, 1900573.
[21] C.-G. Han, X. Qian, Q. Li, B. Deng, Y. Zhu, Z. Han, W. Zhang, W. Wang, S.-P. Feng, G. Chen, W. Liu, *Science* **2020**, *368*, 1091.
[22] Y. Cao, Y. J. Tan, S. Li, W. W. Lee, H. Guo, Y. Cai, C. Wang, B. C. K. Tee, *Nat. Electron.* **2019**, *2*, 75.
[23] Y. Ren, J. Guo, Z. Liu, Z. Sun, Y. Wu, L. Liu, F. Yan, *Sci. Adv.* **2019**, *5*, eaax0648.
[24] Y. M. Kim, H. C. Moon, *Adv. Funct. Mater.* **2020**, *30*, 1907290.

[25] Z. Zhang, T. Chao, L. Liu, G. Cheng, B. D. Ratner, S. Jiang, *J. Biomater. Sci., Polym. Ed.* **2009**, *20*, 1845.
[26] J. Ning, G. Li, K. Haraguchi, *Macromolecules* **2013**, *46*, 5317.
[27] G. Gao, G. Du, Y. Cheng, J. Fu, *J. Mater. Chem. B* **2014**, *2*, 1539.
[28] G. Gao, G. Du, Y. Sun, J. Fu, *ACS Appl. Mater. Interfaces* **2015**, *7*, 5029.
[29] C. Zhao, P. Zhang, J. Zhou, S. Qi, Y. Yamauchi, R. Shi, R. Fang, Y. Ishida, S. Wang, A. P. Tomsia, M. Liu, L. Jiang, *Nature* **2020**, *580*, 210.
[30] K. Haraguchi, K. Uyama, H. Tanimoto, *Macromol. Rapid Commun.* **2011**, *32*, 1253.
[31] J. Yang, R. Bai, B. Chen, Z. Suo, *Adv. Funct. Mater.* **2020**, *30*, 1901693.
[32] H. Yuk, C. E. Varela, C. S. Nabzdyk, X. Mao, R. F. Padera, E. T. Roche, X. Zhao, *Nature* **2019**, *575*, 169.
[33] K. Haraguchi, S. Shimizu, S. Tanaka, *Langmuir* **2018**, *34*, 8480.
[34] T. L. Sun, T. Kurokawa, S. Kuroda, A. B. Ihsan, T. Akasaki, K. Sato, M. A. Haque, T. Nakajima, J. P. Gong, *Nat. Mater.* **2013**, *12*, 932.
[35] S. Pan, F. Zhang, P. Cai, M. Wang, K. He, Y. Luo, Z. Li, G. Chen, S. Ji, Z. Liu, X. J. Loh, X. Chen, *Adv. Funct. Mater.* **2020**, *30*, 1909540.
[36] H. Yuk, T. Zhang, S. Lin, G. A. Parada, X. Zhao, *Nat. Mater.* **2016**, *15*, 190.
[37] J. Li, A. D. Celiz, J. Yang, Q. Yang, I. Wamala, W. Whyte, B. R. Seo, N. V. Vasilyev, J. J. Vlassak, Z. Suo, D. J. Mooney, *Science* **2017**, *357*, 378.
[38] S.-B. Jeon, W.-G. Kim, S.-J. Park, I.-W. Tcho, I.-K. Jin, J.-K. Han, D. Kim, Y.-K. Choi, *Nano Energy* **2019**, *65*, 103994.
[39] S. Yao, Y. Zhu, *Nanoscale* **2014**, *6*, 2345.
[40] S. Gonçalves, J. Serrado-Nunes, J. Oliveira, N. Pereira, L. Hilliou, C. M. Costa, S. Lanceros-Méndez, *ACS Appl. Electron. Mater.* **2019**, *1*, 1678.
[41] M. S. Sarwar, Y. Dobashi, C. Preston, J. K. M. Wyss, S. Mirabbasi, J. D. W. Madden, *Sci. Adv.* **2017**, *3*, e1602200.
[42] Q. Zhang, S. Niu, L. Wang, J. Lopez, S. Chen, Y. Cai, R. Du, Y. Liu, J.-C. Lai, L. Liu, C.-H. Li, X. Yan, C. Liu, J. B.-H. Tok, X. Jia, Z. Bao, *Adv. Mater.* **2018**, *30*, 1801435.